JOURNAL OF AIRCRAFT
Vol. 35, No. 1, January–February 1998

Active Control of Helicopter Blade Stall

Khanh Nguyen*
NASA Ames Research Center, Moffett Field, California 94035

This paper describes the numerical analysis of an automatic stall suppression system for helicopters. The analysis employs a finite element method and includes unsteady aerodynamic effects (dynamic stall) and a nonuniform inflow model. The stall suppression system, based on a transfer matrix approach, uses blade root actuation to suppress stall directly. The results show that stall can effectively be suppressed using higher harmonic blade root pitch at both cruise and high-speed flight conditions. The control amplitude was small, less than 1 deg. In a high-thrust, low-speed flight condition, stall is fairly insensitive to higher harmonic inputs. In general, stall suppression does not guarantee performance improvements. The results also show the distinction between stall suppression and performance improvement with active control. When the controller aims to reduce the shaft torque, rotor performance improvement can be achieved with a small degradation in stall behavior.

Introduction

SUPPRESSION of retreating blade stall has been proposed as a means to expand the helicopter flight envelope, thereby enhancing the utility of these aircraft. Unlike fixed-wing aircraft, stall does not limit the low speed operation of helicopters. Stall on rotor blades, however, limits the helicopter maximum speed as well as the loading capabilities. Stall places a loading limit on most of the helicopter flight envelope at low and medium speed, and at high speed, either stall or compressibility effects can limit helicopter operations. A rotor experiencing stall can require more shaft power than is available from the engine. Also, the excessive control loads on a stalled rotor blade, together with the changes in blade aerodynamic behavior, adversely affect aircraft handling qualities. Stall-induced loads, possibly in combination with blade dynamics as in stall flutter, can severely damage blade structural components and cause excessive cabin vibration.

A unique characteristic of helicopter stall is the occurrence of stall on the retreating side of the rotor disk. In forward flight, a blade encounters a different dynamic pressure as a result of the combination of blade rotation and rotor translation speed. Thus, the dynamic pressure is greater on the advancing side than on the retreating side. For roll moment balance, the blade operates at angles of attack that are low on the advancing side and high on the retreating side. At high blade loading or at high forward speeds, the local blade section angle of attack can become large enough to stall. For untwisted blades, the stall area occurs near the blade tip, growing inboard as the loading or the forward speed increases.[1] For twisted blades, the effects are reversed; the stall area spreads from the blade root outboard.

Operating in an unsteady environment, the most severe type of stall encountered by a rotor blade is dynamic stall. In forward flight, the blade experiences time-varying dynamic pressure and angle of attack arising from blade pitch inputs and elastic responses, and nonuniform rotor inflow. If supercritical flow develops under dynamic conditions, then dynamic stall is initiated by leading-edge or shock-induced separation. Supercritical flow is associated with the bursting of the separation bubble as the bubble encounters the large adverse pressure gradient near the blade leading edge.[2] Dynamic stall is characterized by the shedding of strong vortices from the leading-edge region. The leading-edge vortex produces a large pressure wave moving aft on the airfoil upper surface and creating abrupt changes in the flowfield. The pressure wave also contributes to large lift and moment overshoots in excess of static values and significant nonlinear hysteresis in the airfoil behavior.

The other type of stall typically encountered by rotor blades involves trailing-edge separation. The phenomenon of trailing-edge separation is associated with either static or dynamic conditions. Separation starts from the airfoil trailing edge, and with increasing angle of attack, the separation point progresses toward the leading-edge region. Trailing-edge separation contributes to nonlinear behavior, such as hysteresis, in lift, drag, and pitching moment because of the loss in circulation. In contrast to dynamic stall that is characterized by abrupt changes in airfoil behavior, trailing-edge stall progresses at a moderate rate.

Passive control of blade stall typically involves the tailoring of blade twist and planform for efficient blade load distribution. Another method employs blade construction with multiairfoil sections—thick, high-lift sections inboard and thin, transonic sections for the tip region. These methods aim to provide efficient rotor disk loading and low drag and, thus, are employed primarily for performance benefits; in addition, they provide stall alleviation.

As an alternative to passive methods, active control of blade pitch has the potential to alleviate blade stall. Recent development of high-frequency, blade-mounted actuators[3] makes this concept feasible. The operating frequencies for blade pitch control are not limited by the blade-integer harmonics, as in swashplate oscillation, but by the bandwidth of the actuators. Recently, ZF Luftfahrttechnik, GmbH of Germany built and wind-tunnel tested, together with NASA Ames Research Center, an individual-blade-control system on a full-scale BO-105 rotor. These actuators were tested at harmonics from two to six per-rev (42.5 Hz) and at amplitudes up to 3 deg. Although no stall suppression study was attempted, the benefits of individual blade control (IBC) input on rotor performance at high forward speed (advance ratio $\mu = 0.4$) were encouraging.

Previous Work

In 1952, Stewart[4] suggested that two per-rev (2P) blade pitch applied to rotors in forward flight could be used to delay the

Received June 18, 1996; revision received July 17, 1997; accepted for publication July 28, 1997.

*Aerospace Engineer, Rotorcraft Aeromechanics Branch. Member AIAA.

onset of retreating blade stall. Based on the analysis that included a rigid flapping blade, quasisteady aerodynamics, and uniform inflow models, Stewart derived an approximate transfer function relating the change in 2P blade angle of attack caused by 2P control.[4] Results indicated that rotor disk loading could be efficiently redistributed using higher harmonic blade pitch. For a particular flight condition, the loading redistribution could be adjusted to avoid retreating blade stall. The resulting effect would be to raise the speed limitation of helicopters. According to his analysis, the helicopter speed limit could be increased by 0.1 in advance ratio. However, Stewart did not consider the power requirement caused by the speed increase.

Payne[5] expanded Stewart's results[4] to include the effects of active control using input harmonics higher than 2P. Payne argued that 2P control alone would not be sufficient to raise the speed limitation of helicopters, but a combination of the second and higher harmonic control would be more effective. In the process, he derived generalized transfer functions relating changes in blade angle of attack to the higher harmonic control of a hovering rotor. However, Payne did not quantify the speed limit gain from the approach.

Arcidiacono[6] conducted a numerical simulation to study the effects of second and higher harmonic control on stall. This numerical analysis was more accurate and included more accurate modeling than previous analyses. The analysis was capable of including the effects of static stall and Mach number in the form of two-dimensional airfoil tables. Based on the computed transfer functions relating higher harmonic control to changes in blade angle of attack, Arcidiacono derived a blade pitch schedule that approximated an ideal schedule for stall alleviation. The analysis showed that the blade pitch schedule, which included both 2P and 3P components with a combined maximum amplitude of 4.3 deg, was capable of avoiding retreating blade stall. The resulting effects could raise the speed limit of a helicopter by 30% over the baseline maximum speed. The additional power requirement because of the speed gain would be large, however, to compensate for the increase in fuselage and rotor profile drag (about 100%).

In 1961, a flight-test program was conducted to investigate the benefits of using higher harmonic control on a UH-1A helicopter.[7] Using a rotor head mechanism capable of generating 2P blade pitch, Bell Helicopter conducted a series of flight tests to determine the effects of active control on rotor performance and loads. Test results indicated that the 2P control at different amplitudes and phases did not produce any reduction in rotor shaft torque. Determined to resolve this variance with theoretical prediction, the investigators conducted a post-test analysis. Analytical results indicated that the drag reduction in the retreating side as a result of 2P control was offset by an increase in profile drag in the fore and aft portions of the rotor disk. Such conclusions confirmed previous analytical predictions that 2P control could redistribute the rotor disk loading.

Kretz[8,9] reported the wind-tunnel test results of a stall barrier feedback (SBF) system on a 6-ft-diam two-bladed rotor. The salient feature of the system was the ability to detect and, through feedback control, directly prevent blade stall. The SBF system employed three pressure sensors mounted at the 85% blade radial station and two high-bandwidth hydraulic actuators to control each blade. The pressure sensors provided feedback signals that activated the actuators in an attempt to prevent stall. The system was configured such that once the leading-edge pressure exceeded a threshold value, the actuators became active, generating a sharp pulse, e.g., an 8-deg nose-down pulse was generated within 75 deg of rotor azimuth to reduce the blade pitch. The threshold pressure value had been inferred from two-dimensional airfoil test data and used as an indicator of stall onset. Limited stall avoidance was achieved with the SBF system, resulting in some lift gain. Most significant was the performance gain—an 8% reduction in shaft torque—for the rotor operating at an advance ratio of 0.3 and blade loading C_T/σ of 0.1. However, it was unclear whether the rotor was retrimmed after the application of active control to maintain identical rotor operating conditions.

As a leading advocate in IBC, Ham[10,11] also conducted experiments in active stall suppression. The methods of sensing stall, however, differed from that of Kretz.[8,9] In one experiment, reported by Ham and Quackenbush,[10] the controller fed back and amplified the blade torsion rate to increase blade torsion damping. The increase in damping would prevent stall flutter, an indicator of retreating blade stall. Blade-mounted accelerometers provided information about blade torsion motions. The experiment was conducted in a nonrotating mode and, thus, was not validated in a simulated helicopter environment. In another experiment, Ham[11] reported that the controller successfully reduced 5P blade in-plane accelerations, used as an indicator of retreating blade stall. In contrast to Kretz's method, these two methods control stall indirectly.

Scope of Current Investigation

The objective of the current study is to evaluate the effectiveness of an automatic stall suppression system for helicopters using higher harmonic blade root input. The effects of stall suppression on rotor performance and the control authority required are also investigated.

An advanced rotorcraft analysis, capable of modeling the aeroelastic response of elastic blades, dynamic stall, and nonuniform rotor inflow, is adopted and modified for the active control study. The nonlinear controller development is based on a transfer matrix approach with the option for matrix updating at each controller cycle. The effect of stall reduction on rotor performance is investigated. The results quantify the distinction between control of stall vs control for performance gain.

Two aspects of the present study are unique. First, stall suppression is formulated as an optimization problem in which the stall behavior of a rotor is quantified and subsequently minimized using higher harmonic control (HHC). Thus, the system suppresses stall directly. Second, the range of flight conditions considered varies from low- to high-speed flight, which helps evaluate the effectiveness of higher harmonic control for stall suppression when different physical phenomena dominate the rotor flow field, e.g., low-speed stall vs high-speed shock-induced separation.

In this paper, the term higher harmonic control refers to blade pitch input with harmonic contents greater than 1/rev. Because the focus of this paper is on the aerodynamic performance aspects of stall suppression, the effects of HHC on blade loads, control system loads, and vibratory hub loads, which can be significant, are not discussed.

Description of Analysis

Aeroelastic Analysis

Because accurate representation of the blade aeroelastic responses to the complex rotor flowfield, together with a robust and accurate numerical method for blade response solution, is mandatory for the analysis of stall control, the Ames-modified version of the University of Maryland Advanced Rotorcraft Code (UMARC)[12] is adopted for this investigation. UMARC/A is a finite element code that includes advanced unsteady aerodynamics and vortex–wake modeling. The structural and aerodynamic modeling of UMARC/A makes the code a suitable analysis for studying active control effects on rotor behavior.

The rotor blade is modeled as an elastic, isotropic Bernoulli–Euler beam undergoing small strain and moderate deflections. The blade degrees of freedom are flap bending, lead-lag bending, elastic twist, and axial deflections. The finite element-method based on Hamilton's principle allows a dis-

cretization of the blade model into a number of beam elements, each with 15 deg of freedom.

The blade airloads are calculated using a nonlinear unsteady aerodynamic model proposed by Leishman and Beddoes.[13] This model consists of an attached compressible flow formulation along with a representation of the nonlinear effects caused from trailing-edge separation and dynamic stall. In the attached flow formulation, the normal force (or lift) and pitching moment includes both circulatory and impulsive (noncirculatory) components. Physically, the circulatory components model the shed wake effects, while the impulsive components originate from the pressure wave generated by the airfoil motion. For dynamic stall modeling, an artificial normal force c'_N is computed based on the attached flow lift and the dynamics of the pressure distribution, represented by a time-lag model. This quantity incorporates the effects of stall delay and is used as a criterion of stall onset.

The trailing-edge separation model is based on Kirchhoff's formulation, which relates the separation location f to the airfoil force and moment behavior. The variation of the separation location with angle of attack is constructed from static airfoil data, then the results are curve-fitted. The value of the separation location is a measure of the degree of nonlinearity in the lift behavior. Information about the flow separation point also allows the reconstruction of the airfoil static behavior, a precursor to the modeling of the airfoil dynamic characteristics.

For dynamic stall, stall onset is based on the criterion that leading-edge separation initiates only when the artificial normal force c'_N attains a critical value c_{N1}, corresponding to a critical leading-edge pressure. In this model, c_{N1} is the airfoil maximum static lift coefficient (available from airfoil tables) and is a function of the Mach number. Once initiated, the excess lift because of dynamic stall is governed by the dynamics of the vortex lift, defined as the difference in lift between the attached (linear) and separated flow (nonlinear) regimes. The vortex movement over the airfoil upper surface induces a large change in the pitching moment. The vortex-induced pitching moment is computed based on the vortex lift and the position of the c.p.

For the inflow calculation, a prescribed wake model is used for the high-speed flight condition, and a modified free-wake model is used for the low-speed flight condition. Both wake models are adapted from CAMRAD.[14] A modification to the free-wake model improves the convergence behavior of the wake geometry computation by using a predictor–corrector updating scheme with nonreflective periodic boundary conditions.

The coupled blade response and trim control settings are solved for simulated wind-tunnel conditions. For trim, the rotor shaft orientation is prescribed, and the blade collective and cyclic pitch inputs are automatically adjusted to desired values of thrust and hub moments. A modal reduction technique is employed in the blade response solution to reduce the computational requirement. The modal equations are solved iteratively using a robust finite-element-in-time method in which the periodic boundary conditions are inherent in the formulation. The converged solution satisfies the governing equations for both rotor trim and blade response, which include higher harmonic control effects.

Higher Harmonic Control System

The controller algorithm, based on a transfer function matrix approach, is implemented in UMARC/A. Depending on the control objectives considered—to suppress stall or to reduce rotor shaft torque—each element of the transfer matrix represents the sensitivity of the controlled parameter z to each harmonic of the blade root actuation u. In this investigation, the transfer matrix is computed using a finite difference method in which each harmonic of the control input (sine and cosine components) is perturbed individually. The control law is formulated as an optimization problem:

$$\min(qz_i^2 + u_i^T R u_i) \tag{1}$$

subjected to

$$z_i = z_{i-1} + (1 - r)T_i(u_i - u_{i-1}) \tag{2}$$

In Eq. (1), the parameters q (a scalar) and R (a diagonal matrix) assign relative weightings to the controlled parameter z_i and each component of the input vector, respectively.

For stall suppression, z_i is the stall index computed at each controller cycle by

$$z_i = \sum_{m}^{24} \sum_{n}^{120} F(r_m, \psi_n) \tag{3}$$

where the double summation is over the 2880 airload computation points over the rotor disk (24 points in the radial direction $\times$ 120 azimuth steps), and

$$F(r, \psi) = \begin{cases} (c'_N - c_{N1})M^2 & \text{if } c'_N \geq c_{N1} \\ 0 & \text{otherwise} \end{cases} \tag{4}$$

Note that F is defined over the rotor disk, with r being the blade radial station and ψ the azimuth angle. With this definition, the stall index is a metric that measures the severity of stall on the rotor disk in terms of the excess lift over the stall area. The excess lift is the amount of artificial lift c'_N over the airfoil maximum lift c_{N1}, adapted from the dynamic stall model described earlier.

In Eq. (2), the control rate factor r, with a value between 0 and 1, limits the control update rate, and i denotes the controller cycle. The transfer matrix updating is an option in which T_i is updated at each controller cycle, based on a secant method.[15] The T matrix updating, when used in combination with the control rate limit, helps improve the convergence of the controller when nonlinear effects dominate. This approach was successfully applied to another control problem—vibration suppression of rotors under stalled conditions[16]—with significant nonlinearity in the model.

The vector $\boldsymbol{u}_i$ represents the control input that includes harmonics from 2 to 6/rev:

$$\boldsymbol{u}_i = [\theta_{2c}\ \theta_{2s} \cdots \theta_{6c}\ \theta_{6s}]^T \tag{5}$$

In terms of the elements of $\boldsymbol{u}_i$, the higher harmonic schedule for the jth blade is

$$\theta^j_{\text{HHC}}(\psi) = \sum_{k=2}^{6} A_k \cos(k\psi^j - \phi_k) \tag{6}$$

where the amplitude is

$$A_k = \sqrt{\theta_{k,c}^2 + \theta_{k,s}^2} \tag{7}$$

and the phase is

$$\phi_k = \tan^{-1}(\theta_{k,s}/\theta_{k,c}) \tag{8}$$

Besides stall suppression, a second controller is also investigated. This controller aims to improve the rotor performance using higher harmonic blade root pitch. For this system, the controlled parameter [Eq. (3)] is simply the rotor shaft torque. Except for the change in the definition of z, this controller retains the same structure as that of the stall suppression controller. Note that this controller does not restrict the input har-

monic to 2P as in other investigations (such as Refs. 3 or 17), but includes a wider range of input harmonics (2P–6P).

Rotor Model

The rotor model used in the study is a variation on the four-bladed hingeless rotor of the BO-105 helicopter. To better capture the effects of stall control on modern rotors, two modifications are made to the baseline BO-105 rotor: 1) the HH-10 airfoil is used instead of the NACA 23012, and 2) blade linear twist is decreased from −8 to −10 deg. Besides these modifications, the blade geometry and structural properties are essentially the same as for the BO-105 rotor blade. The major characteristics of the rotor model are listed as follows: number of blades, 4, radius 16.11 ft, tip speed 715 ft/s, tip Mach number 0.6334, chord 10.63 in., solidity ratio 0.0701, root cutout 3.7 ft, linear twist −10, precone 2.5 deg, lock number 5.40, airfoil HH-10, and computed blade frequencies (425 rpm, per rev) = first lag 0.71, first flap 1.125, second flap 2.82, first torsion 3.68, second lag 4.53, and third flap 5.10.

Results and Discussion

Validation of Analysis

Results of the individual-blade-control test[3] provide a unique database to validate the analysis, because the data include the effects of active control on a stalled rotor. Analytical results are compared with test data for the following conditions: 85 kn tunnel speed (0.2 advance ratio), 2.1 deg forward shaft tilt, and 8450 lb thrust (1.75g). During the test, a sharp increase in the peak-to-peak pitch link load was used as an indication of stall. Note that stall increased this component of the pitch-link load by 2.5 times from an unstalled condition. Figure 1 shows the effects of a 2P phase sweep on the rotor shaft power. Initially, the phase sweep was conducted at 1-deg amplitude; however, structural load limits on the rotor hardware forced a reduction in the amplitude to 0.3 deg. Test data show two half-sinusoidal variations caused by the 2P phase sweep, and the overall variation indicates a maximum power reduction occurring in the range of 150–210 deg phase angle. Analytical results capture these two variations well. For the 1-deg sweep, the correlation between test data and analytical results is excellent. At 0.3-deg sweep, the analysis computes the correct magnitude in power variation but misses the phase by roughly 30 deg. These results provide confidence in the ability of the analysis to predict rotor behavior under stalled conditions.

Flight Conditions in Active Control Simulations

Simulated flight conditions with significant blade stall are selected at several forward speeds. These include a low-speed condition at 63 kn (μ = 0.15, C_T/σ = 0.16), cruise-speed condition at 127 kn (μ = 0.3, C_T/σ = 0.13), and a high-speed condition at 148 kn (μ = 0.35, C_T/σ = 0.12). For all flight conditions, the steady hub moments are trimmed to zero.

Open-Loop Study

An open-loop study is performed to evaluate the sensitivity of the stall index to the amplitude and phase variation of single harmonic inputs. The approach consists of a phase variation of an input harmonic at a fixed amplitude and a subsequent amplitude variation about an optimum phase where the controlled parameter is at a minimum. These results provide insight into the input–output behavior of the control system and

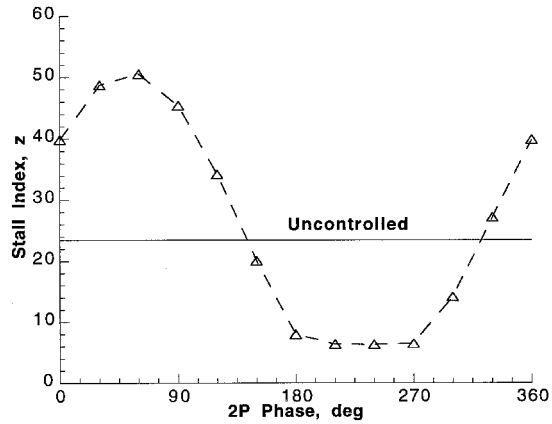

Fig. 2 Variation of stall index with 2P phase angle, 1 deg amplitude (μ = 0.3, C_T/σ = 0.13).

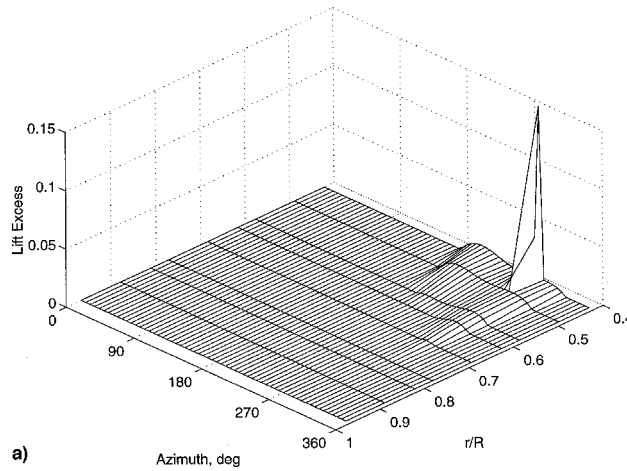

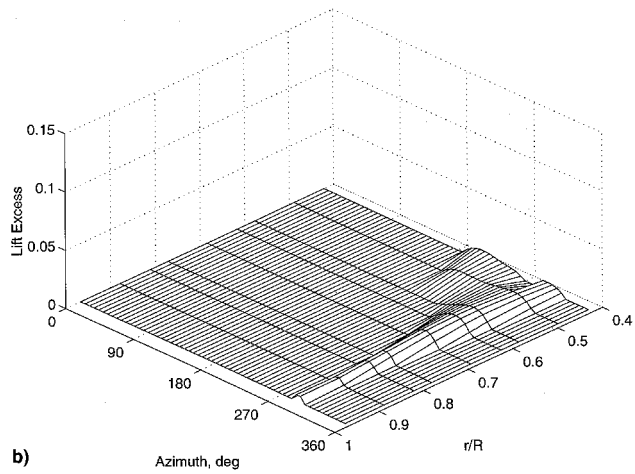

Fig. 3 Evolution of stall over rotor disk: a) uncontrolled and b) 2P phase of 240 deg at 1 deg amplitude (μ = 0.3, C_T/σ = 0.13).

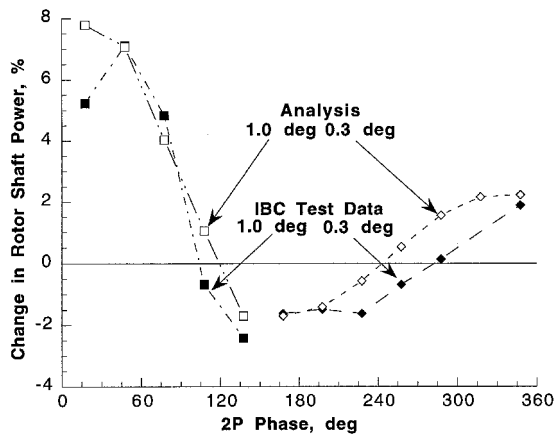

Fig. 1 Comparison of IBC test data with analytical results of a 2P phase sweep on rotor power (μ = 0.2, C_T/σ = 0.125).

help define the type of controller (linear vs nonlinear) to use. The effectiveness of the closed-loop system is also estimated based on open-loop data. Representative results are presented in this paper.

Figure 2 shows the variation of the stall index z as a result of a 2P phase sweep at 1-deg excitation for the cruise-speed flight condition ($\mu = 0.3$, $C_T/\sigma = 0.13$). The results indicate that the stall index varies almost linearly at this amplitude of 2P excitation. Because the range of phase for minimum stall is between 180 and 270 deg, the 2P pitch schedule for stall reduction peaks at two regions of the rotor azimuth, one between 90 and 135 deg and the other between 270 and 315 deg. This result is rather counterintuitive because Fig. 3a, which shows the plot of the excess lift [F in Eq. (4)] over the rotor disk, indicates that stall occurs between 270 and 300 deg azimuth. Interestingly, Fig. 3b, which shows the stall behavior at 240 deg of 2P phase, indicates that the rotor is almost stall-free. These results imply that the blade aeroelastic response to higher harmonic input is an important consideration in stall suppression for helicopters.

The effects of 2P amplitude variation at 240 deg phase on the stall index are shown in Fig. 4 for the cruise-speed flight condition. The results indicate that the stall index increases with 2P amplitude above 1 deg at this phase angle. Curve-fitting the results indicates an optimum amplitude of roughly 0.9 deg at this phase angle.

For the 2P phase sweep at the same operating condition, the shaft torque variation exhibits a different trend than that of the stall index. The results are shown in Fig. 5. Although the relative change in shaft torque is small compared to the change in stall index, a 2% reduction in shaft torque is, however, a significant gain in rotor performance. While minimum stall index occurs in the range of 180–270 phase angle (Fig. 2), minimum torque is at 30 deg phase. In fact, in the phase region where stall index is minimum (180–270 deg), the rotor shaft torque increases above the uncontrolled value and even reaches a maximum at 210 deg phase. An explanation of this phenomenon is provided by an investigation of Fig. 6. Figures 6a–6c show the evolution of the blade drag coefficient over the rotor disk for the baseline case, minimum stall index case, and minimum shaft torque case, respectively. The results show that the drag behavior along the entire blade span shown in the region near 300-deg azimuth is responsible for this phe-

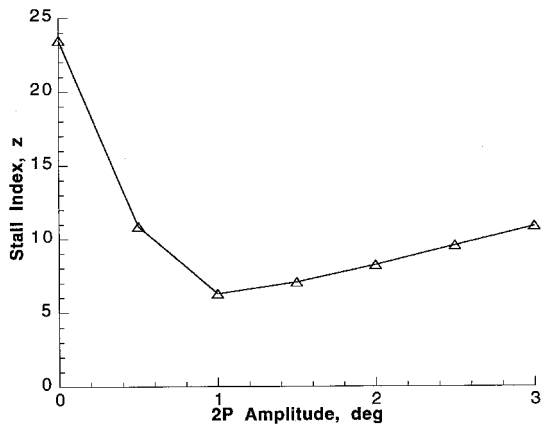

Fig. 4 Variation of stall index with 2P amplitude at 240 deg phase ($\mu = 0.3$, $C_T/\sigma = 0.13$).

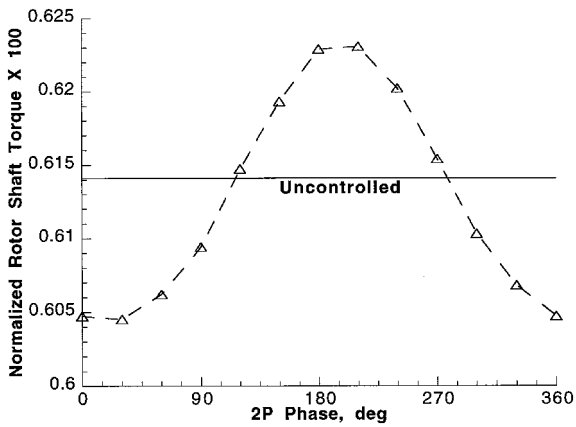

Fig. 5 Variation of shaft torque with 2P phase angle, 1 deg amplitude ($\mu = 0.3$, $C_T/\sigma = 0.13$).

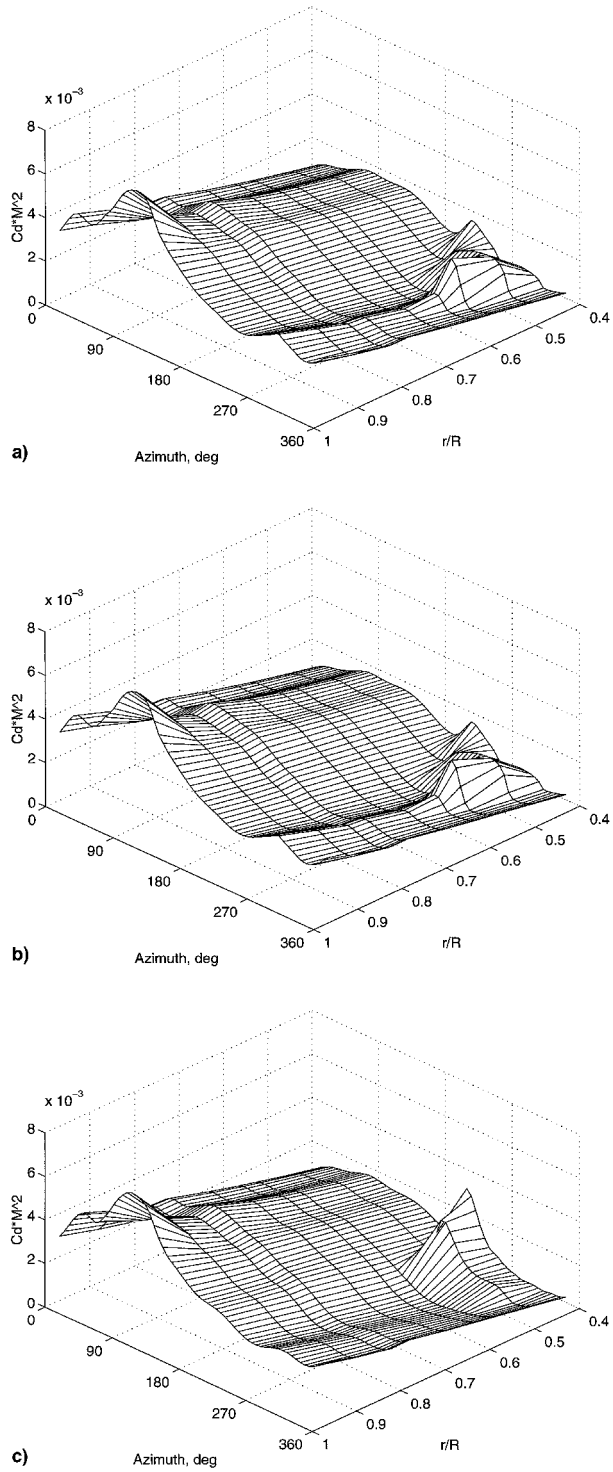

Fig. 6 Evolution of blade drag over rotor disk: a) uncontrolled, b) minimum stall (2P phase 240 deg), and c) minimum torque (2P phase 60 deg) ($\mu = 0.3$, $C_T/\sigma = 0.13$).

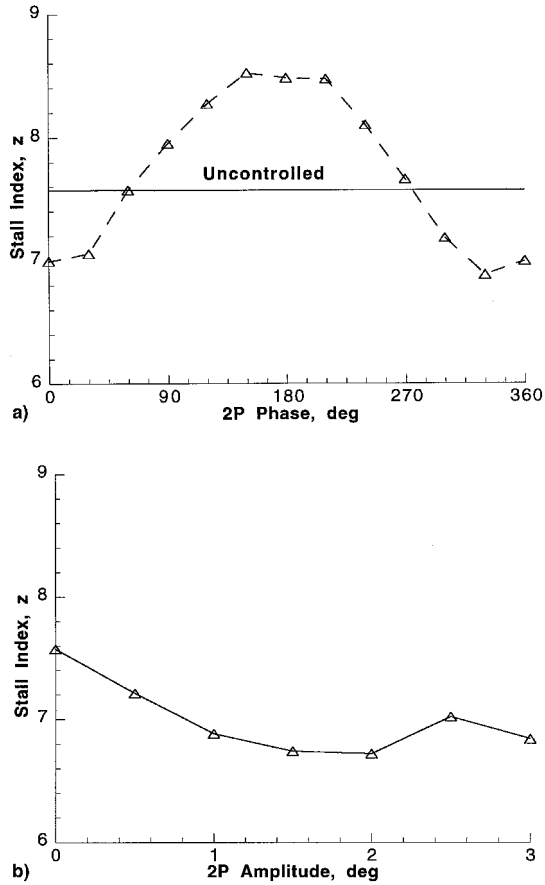

Fig. 7 Variation of stall index with a) 2P phase angle, 1 deg amplitude, and b) 2P amplitude at 330 deg phase (μ = 0.15, C_T/σ = 0.16).

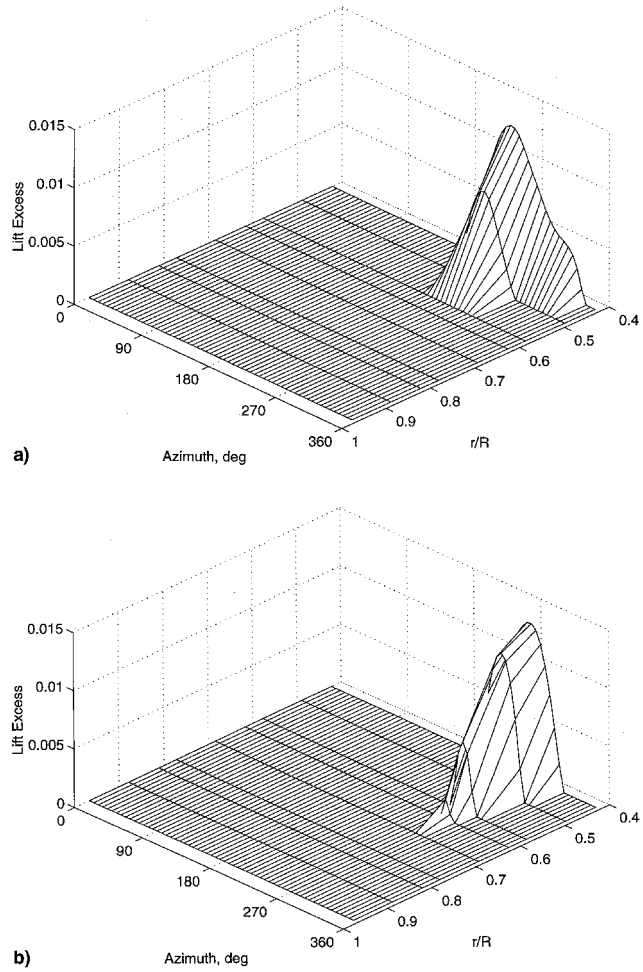

Fig. 8 Evolution of stall over rotor disk: a) uncontrolled and b) multiharmonic control (μ = 0.15, C_T/σ = 0.16).

nomenon. Of the three cases shown, the minimum stall index case has the highest drag rise, while minimum torque has a drag reduction from the baseline. Because the stall area is localized inboard, reducing stall does not guarantee an improvement in rotor performance.

Open-loop results for the low-speed flight condition (μ = 0.15, C_T/σ = 0.16) are shown in Fig. 7. The sensitivity of the stall index to 2P excitation is weak. Figure 7a shows that the stall index varies by only 20% with the 2P phase sweep at 1-deg amplitude. The shaft torque variation with the same phase sweep is moderate, however, varying by 6% about the uncontrolled value. The amplitude variation at the phase for minimum stall index (330 deg), shown in Fig. 7b, exhibits the same low sensitivity. At this low-speed condition, the stall index can be reduced, at best, by only 10% with 2 deg of 2P input. Open-loop results for other harmonics show similar results—the stall index is fairly insensitive to higher harmonic control at this low-speed flight condition.

Closed-Loop Study

Closed-loop results for the low-speed flight condition (μ = 0.15, C_T/σ = 0.16) are presented first. Input harmonics from 2P to 4P are used; the 5P and 6P components are found to destabilize closed-loop operation at this flight condition. The controller reduces the stall index by 17%, with a control amplitude (rms value) of 0.6 deg. The stall behavior for the uncontrolled and controlled cases is shown in Figs. 8a and 8b, respectively. Compared to the uncontrolled case, the controlled excess lift (stall) region is narrower in the azimuth range, yet protrudes slightly outboard. For this flight condition, the stall index reduction is accompanied by an 8.5% reduction in shaft torque. The input for stall suppression at this flight condition is shown as case 1 in Table 1.

For the cruise-speed flight condition (μ = 0.3, C_T/σ = 0.13), the controller uses input harmonics from 2P to 6P. The stall index is reduced by over 75%, and the control amplitude is only 0.37 deg. Table 1 shows the amplitudes and phases of the blade pitch harmonics (case 2). For the same flight condition, the open-loop results shown previously indicate that the same level of stall alleviation can be achieved with 1.0 deg of 2P input, and yet the shaft torque increases. For the multiharmonic case, however, the reduction in stall is accompanied by a 0.5% reduction in shaft torque. With multiharmonic inputs, Fig. 9 shows that stall can be reduced without increasing the blade drag in the azimuth region of 300 deg (compare Fig. 9 with Figs. 6a and 6b).

The effectiveness of closed-loop operation using only 2P is evaluated. The controller converges to a minimum stall index using 0.85 deg of control amplitude at 220 deg phase (Table 1, case 3). The reduction in stall is similar to the multiharmonic cases, achieving a 74% reduction in stall index. As in the open-loop results, the 2P input increases the rotor shaft torque by 2.3%. For stall suppression, multiharmonic inputs are more efficient than 2P input in terms of control amplitude requirement. Furthermore, the multiharmonic input incurs no performance penalty.

Closed-loop control with multiharmonic input is also effective at the high-speed condition (μ = 0.35, C_T/σ = 0.12). Because the system exhibits moderately nonlinear behavior, this is the only flight condition that requires transfer matrix updating. The stall index is reduced by 75% using 0.8 deg of control amplitude (see Table 1, case 4). Figures 10a and 10b show the stall behavior for the uncontrolled and controlled cases, respectively. All of the stall areas, except for the one at the

Table 1 Closed-loop results

Cases	Flight conditions	A_2; ϕ_2 (deg)	A_3; ϕ_3 (deg)	A_4; ϕ_4 (deg)	A_5; ϕ_5 (deg)	A_6; ϕ_6 (deg)	ΔStall index, %	ΔShaft torque, %
1	Low speed	0.10; −13	0.37; 112	0.98; −99	——	——	−17	−8.5
2	Cruise	0.12; −140	0.08; 77	0.05; −143	0.11; 35	0.32; 125	−75	−0.5
3	Cruise	0.85; −140	——	——	——	——	−74	2.3
4	High speed	0.26; 117	0.30; 1	0.05; 180	0.47; −24	0.51; 125	−75	−6
5	Cruise	0.04; −56	0.23; 132	0.39; 31	0.09; 32	0.13; 13	1	−5

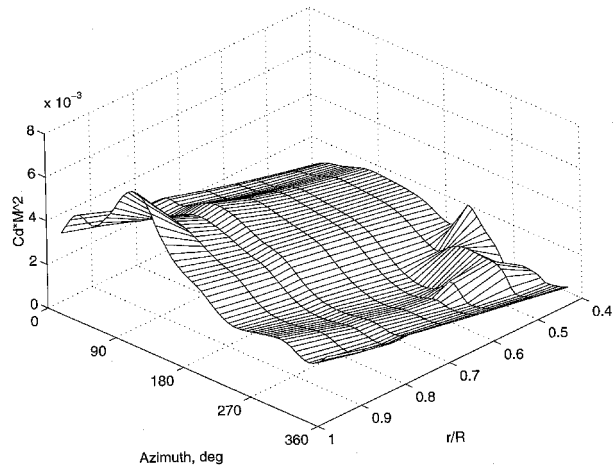

Fig. 9 Evolution of blade drag over rotor disk with multiharmonic control (μ = 0.3, C_T/σ = 0.13).

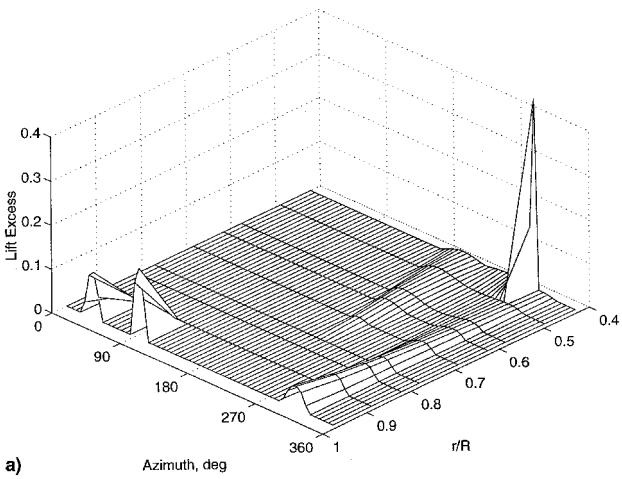

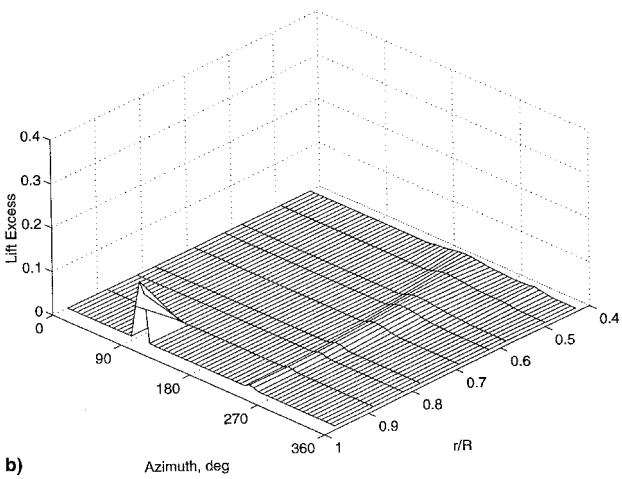

Fig. 10 Evolution of stall over rotor disk: a) uncontrolled and b) multiharmonic control (μ = 0.35, C_T/σ = 0.12).

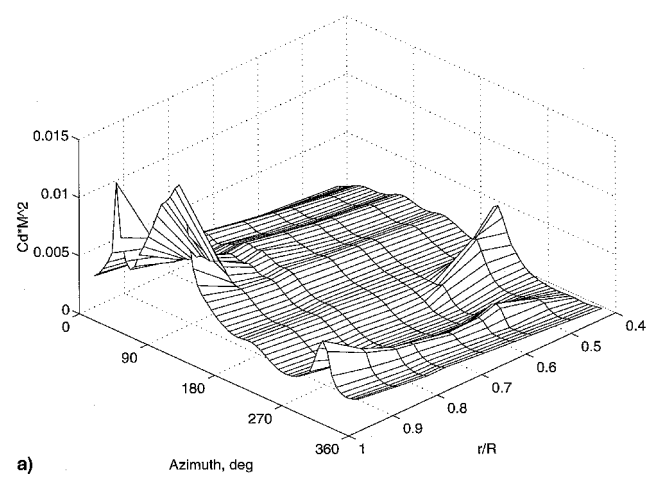

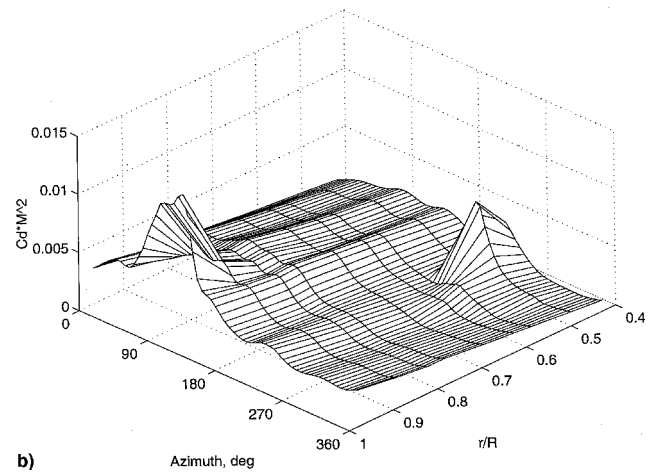

Fig. 11 Evolution of blade drag over rotor disk: a) uncontrolled and b) multiharmonic control (μ = 0.35, C_T/σ = 0.12).

advancing blade tip region, are suppressed. The blade drag plots of Fig. 11 show that the controller is capable of relieving most of the drag rises over the rotor disk, resulting in a 6% reduction in the rotor shaft torque.

Control for Performance Gain

For this part of the study, the rotor shaft torque is the controlled parameter. The cruise-speed flight condition is considered (μ = 0.3, C_T/σ = 0.13). The controller employs a multiharmonic input including 2P to 6P components. The controller reduces the shaft torque by 5%. The maximum control authority was roughly 0.6 deg with the 3P and 4P components dominant (see Table 1, case 5). The stall index, however, increased by 1%. A comparison of two multiharmonic waveforms—one for stall suppression (case 2) and one for torque reduction (case 5)—at the same flight condition is shown in Fig. 12. For performance improvement, the input requirement is global, encompassing many different phenomena such as loading distribution, retreating blade stall, and advancing blade compressibility. On the other hand, the require-

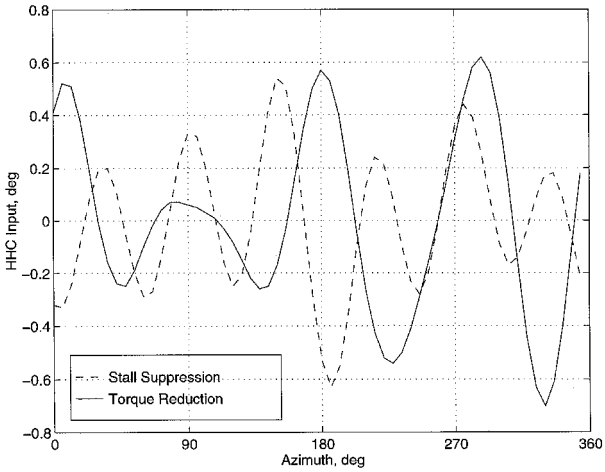

Fig. 12 Comparison of HHC schedules for stall suppression and for torque reduction ($\mu = 0.3$, $C_T/\sigma = 0.13$).

ment for stall suppression is local, focusing only on the stall region on the retreating side.

Concluding Remarks

The results of this investigation demonstrate that stall can be suppressed effectively with higher harmonic control at both cruise- and high-speed flight conditions. The control amplitude requirements are less than 1 deg. However, because stall is only one of the phenomena affecting rotor performance, the suppression of stall, as implemented here, does not guarantee a gain in rotor performance.

In low-speed flight, open-loop results indicate that the stall index was fairly insensitive to higher harmonic input. Although the reduction in stall index was small with closed-loop multiharmonic control, a sizable gain in rotor performance was achieved.

The blade pitch schedule that improved rotor performance was different from the one that suppressed stall for the cruise-speed flight condition. Rotor performance improvement can be achieved with a small degradation in stall behavior.

Acknowledgments

The author would like to thank Steve Jacklin for providing the test data presented in Fig. 1.

References

[1]Gessow, A., and Myers, C., *Aerodynamics of the Helicopter*, Frederick Ungar, New York, 1981, pp. 250–267.

[2]McCroskey, W. J., Carr, L. W., and McAlister, K. W., "Dynamic Stall Experiments on Oscillating Airfoils," *AIAA Journal*, Vol. 14, No. 1, 1976, pp. 57–63.

[3]Jacklin, S., Nguyen, K., Blaas, A., and Richter, P., "Full Scale Wind Tunnel Test of a Helicopter Individual Blade Control System," *Proceedings of the 50th Annual Forum of the American Helicopter Society*, American Helicopter Society, Alexandria, VA, 1994, pp. 579–596.

[4]Stewart, W., "Second Harmonic Control on the Helicopter Rotor," Aeronautical Research Council, RM-2997, London, Aug. 1952.

[5]Payne, P. R., "Higher Harmonic Rotor Control," *Aircraft Engineering*, Vol. 30, No. 354, 1958, pp. 222–226.

[6]Arcidiacono, P. J., "Theoretical Performance of Helicopters Having Second and Higher Harmonic Feathering Control," *Journal of the American Helicopter Society*, Vol. 6, No. 2, 1961, pp. 8–19.

[7]Drees, J. M., and Wernicke, R. K., "An Experimental Investigation of a Second Harmonic Feathering Device on the UH-1A Helicopter," U.S. Army Transportation Research Command, TR-62-109, Fort Eustis, VA, June 1963.

[8]Kretz, M., "Active Eliminating of Stall Conditions," *Proceedings of the 37th Annual Forum of the American Helicopter Society*, American Helicopter Society, Alexandria, VA, 1981, pp. 18–25.

[9]Kretz, M., "Active Expansion of Helicopter Flight Envelope," *Proceedings of the 15th European Rotorcraft Forum*, 1989, pp. 53.1–53.18 (Paper 53).

[10]Ham, N., and Quackenbush, T., "A Simple System for Helicopter Individual-Blade-Control and Its Application to Stall Flutter Suppression," *Proceedings of the 7th European Rotorcraft Forum*, 1981, pp. 76.1–76.9 (Paper 76).

[11]Ham, N., "Helicopter Stall Alleviation Using Individual-Blade-Control," *Proceedings of the 10th European Rotorcraft Forum*, Aug. 1984, pp. 50A.1–50A.4 (Paper 50).

[12]Chopra, I., and Gunjit, S. B., "University of Maryland Advanced Rotor Code: UMARC," *Proceedings of the Aeromechanics Specialists Conference*, American Helicopter Society, Alexandria, VA, 1994, pp. PS.5.1–PS.5.31 (Paper PS.5).

[13]Leishman, J. G., and Beddoes, T. S., "A Semi-Empirical Model for Dynamic Stall," *Journal of the American Helicopter Society*, Vol. 34, No. 3, 1989, pp. 3–17.

[14]Johnson, W., "A Comprehensive Analytical Model of Rotorcraft Aerodynamics and Dynamics, Part I: Analysis and Development," NASA TM-81182, June 1980.

[15]Dennis, J. E., Jr., and Schnabel, R. B., *Numerical Method for Unconstrained Optimization and Nonlinear Equations*, Prentice–Hall, Englewood Cliffs, NJ, 1983, pp. 168–193.

[16]Nguyen, K., and Chopra, I., "Application of Higher Harmonic Control to Rotors Operating at High Speed and Thrust," *Journal of the American Helicopter Society*, Vol. 35, No. 3, 1990, pp. 78–89.

[17]Nguyen, K., and Chopra, I., "Effects of Higher Harmonic Control on Rotor Performance and Control Loads," *Journal of Aircraft*, Vol. 29, No. 3, 1992, pp. 336–342.